Journal of MATERIALS RESEARCH

Article
DOI: 10.1557/jmr.2019.6

Modified carbon nanotubes for water-based cathode slurries for lithium–sulfur batteries

Olesya O. Kapitanova[1,a], Kirill V. Mironovich[1], Daniil E. Melezhenko[1], Viktoria V. Rokosovina[1], Serafima Y. Ryzhenkova[1], Sergey V. Korneev[1], Tatyana B. Shatalova[1], Xieyu Xu[1], Filipp S. Napolskiy[2], Daniil M. Itkis[3], Victor A. Krivchenko[4]

[1]*Moscow State University, Moscow 119991, Russia*
[2]*Dubna University, Dubna 141980, Russia*
[3]*Moscow State University, Moscow 119991, Russia; and Dubna University, Dubna 141980, Russia*
[4]*Moscow State University, Moscow 119991, Russia; and Institute of Arctic Technology of MIPT, Dolgoprudny, Moscow Region 141701, Russia*
[a)]Address all correspondence to this author. e-mail: olesya.kapitanova@gmail.com

Received: 9 October 2018; accepted: 27 December 2018

In this study, for the first time, chemically modified carbon nanotubes (CNTs) were used as a conductive additive in the cathode composite for lithium–sulfur batteries. Oxidation of pure CNTs has been carried out using modified Hummers' method, and to partially remove oxygen groups from the CNT surface and increase their electronic conductivity, oxidized CNTs have been hydrothermally treated. The cathode slurry was mixed in water with a water-soluble LA133 binder. Despite the decrease in electronic conductivity of CNTs after chemical treatment, the presence of structural defects and oxygen groups provides uniform distribution of modified CNTs in the sulfur-based composite, which results in more than twice higher electrode specific capacity compared with the electrodes comprising pure CNTs. Using chemically modified CNTs as a conductive additive is proposed as an effective way for the preparation of nontoxic and cost-effective water-based cathode slurries in lithium–sulfur batteries.

Introduction

Sulfur is considered as a cathode material with an extremely high specific capacity (1700 mA h/g) [1, 2, 3]. A system employing a sulfur cathode and lithium metal anode has a high theoretical specific energy of 2500 W h/kg of active components [1, 2]. According to some estimations, practical specific energy of Li–S battery can exceed 600 W h/kg [4], which is significantly higher than that of lithium-ion cells. One of the main factors hampering practical implementation of lithium–sulfur batteries is the complexity of the reactions occurred in the cathode during the discharge/charge process and associated with the formation of lithium polysulfides (Li_2S_n) [1, 2, 5, 6, 7]. The solubility of higher polysulfides ($6 < x \leq 8$) in the electrolyte leads to so-called polysulfide "shuttle" in the battery, which has a very negative impact on the system efficiency.

A number of methods have been developed to provide encapsulation of polysulfide in a polar matrix based on polymers, graphene-based materials, metal chalcogenides and oxides [8], metal–organic frameworks [9, 10, 11], and mediators [12, 13, 14] to suppress the polysulfide "shuttle" and improve the Coulombic efficiency of sulfur-based cathodes [15].

Moreover, the low electronic conductivity of sulfur ($\sim 10^{-30}$ S/cm) and Li_2S requires insertion of conductive additives to cathode structure to increase utilization of an active material and improve battery cycle life [15]. Carbon nanotubes (CNTs) along with graphene are very attractive conductive additives to anchor sulfur in lithium–sulfur battery cathodes and increase mechanical strength of an electrode coating [1, 16, 17, 18, 19]. However, effective use of CNT powders in cathode slurries demands dispersion of CNT agglomerates. Problem of a CNT agglomeration may be especially crucial in water, since pure CNTs demonstrate hydrophobic behavior.

Oxidation of CNTs leads to the formation of various oxygen-containing groups, such as hydroxyl, aldehyde, ketone, ether, carboxyl, anhydride, and lactone, on the surface of CNT [4, 20]. Such groups enable a polar interaction between carbon additive surface and polysulfides, leading to suppression of polysulfide shuttle [21, 22, 23, 24].

https://doi.org/10.1557/jmr.2019.6 Published online by Cambridge University Press

© Materials Research Society 2019

Also, little amount of oxygen-containing surface groups makes possible interaction of modified CNTs with polar solvents, such as water, and aqueous binder [25, 26, 27], resulting in their uniform volume distribution during cathode slurry preparation. This allows to exclude toxic and expensive organic solvent *N*-methyl-2-pyrrolidone (NMP) from technological process of cathode fabrication [15].

In this study, we used chemically modified CNTs as a conductive additive in the cathode composite for lithium–sulfur batteries. The modification process included chemical oxidation of the CNTs, followed by hydrothermal reduction. Such approach led to significant disorder of the CNT structure, creating a large number of defects and maintaining, at the same time, the linear morphology of the conducting additive. It also allowed to accurately control the amount of residual oxygen groups on the surface.

The cathode slurry was mixed in water with a water dispersion of acrylonitrile multi-copolymer LA133. It was shown that using modified CNTs enables to increase the utilization of sulfur in the cathode more than twice compared with pristine CNTs. Despite the decrease in CNT electronic conductivity after chemical treatment, the presence of structural defects and oxygen groups provides uniform CNT distribution in the sulfur-based composite, which results in higher electrode specific capacity.

Results and discussion

Enhancing the adhesion between conductive carbon additive and the sulfur-containing active material [composite of graphene oxide (GO) and sulfur particles] can be achieved by enabling a polar interaction between these components in the cathode slurries. To introduce structural defects and surface functional groups, CNTs were first chemically oxidized and further partially reduced.

We controlled the efficiency of CNT oxidation and subsequent partial reduction using IR (infrared) spectroscopy. Fig. 1 shows the IR spectra of the CNTs after oxidation (a) and further hydrothermal reduction during one (b) and four hours (c). After CNT oxidation, a number of vibrations from oxygen-containing functionalities are clearly seen [28, 29]: C=O stretching (≈1674–1776 cm^{-1}), COOH/O–H stretching (≈3600–2800 cm^{-1}), H–O–H deformation (1644 cm^{-1}), O–H deformation (1408 cm^{-1}), and C–O stretching (number of peaks in the range of 1332–1039 cm^{-1}).

Hydrothermal treatment has led to almost complete elimination of carboxyl and hydroxyl groups and intercalated and adsorbed water. Intensities of the lines ascribed to carbonyl and ether stretching vibrations significantly decreased. C–O vibrations in the range 1332–1039 cm^{-1}, which were easily distinguishable before reduction, can not be resolved after

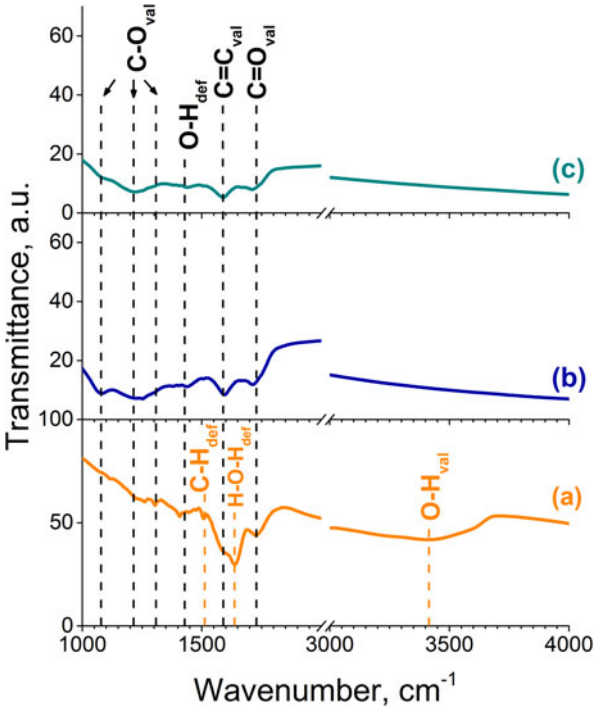


Figure 1: IR spectra of oxidized SWCNTs before (a) and after 1 (b) and 4 (c) hours of hydrothermal reduction. IR spectrum of SWCNT and IR spectra in full scale are presented in Supplementary material (Fig. S1).

hydrothermal treatment due to broadening and decreased intensity. The appearance of a peak corresponding to the aromatic system (stretching $C = C_{val}$ 1588 cm^{-1}) indicates a partial regeneration of the π-system after the reduction of the oxidized CNTs.

Ultraviolet (UV)–visible absorption spectroscopy further confirmed that hydrothermal treatment results in strong reduction of oxidized CNTs. Noticeable red shift of the absorption band (from 238 to 254 nm) is clearly seen in Fig. 2(a) for hydrothermally treated CNTs, which indicates restoration of the electronic conjugation in the nanotubes [20, 30]. It is also indirectly confirmed by the decreased relative transmittance of both IR and visible light after the reduction. Strong IR absorption is typical for CNTs (see Fig. S1 in Supplementary material).

Raman analysis further helped in deeper understanding of the effect of modification on the level of disorder of the CNTs. It is well known that Raman spectroscopy is a sensitive tool to reveal the structure and electronic properties of CNTs [31]. A number of parameters, like G/D intensity ratio, radial breathing mode (RBM), and G mode position and lineshape, are sensitive to CNT structural features, i.e., its diameter, electronic structure (metallic and semiconducting), and defects of different nature [31]. The G mode is ascribed to a first-order process associated with vibrations between the two dissimilar carbon atoms A and B in the unit cell. For pristine CNTs, the G mode

https://doi.org/10.1557/jmr.2019.6 Published online by Cambridge University Press

© Materials Research Society 2019

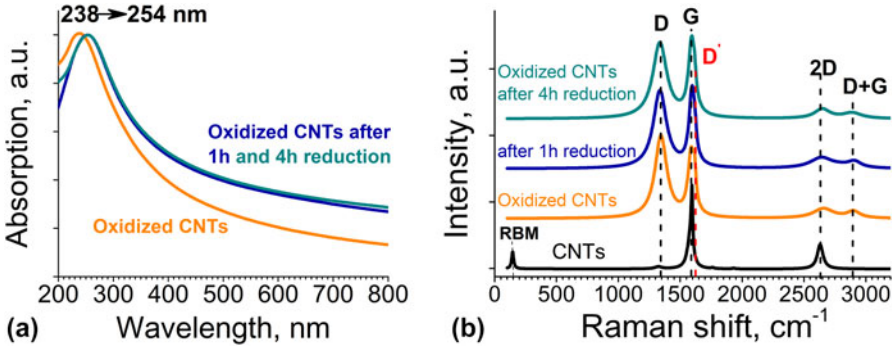


Figure 2: (a) UV–visible spectra and (b) Raman spectra of SWCNTs, oxidized CNTs, and CNTs after reduction.

around 1580 cm^{-1} splits into G^+ and G^- modes [Fig. 2(b)] due to the phonon wave vector confinement along the SWCNT circumferential direction and due to symmetry-breaking effects associated with SWCNT curvature [31]. The 2D mode arises from a two-phonon, intervalley, second-order Raman scattering process. Comparable intensity of 2D and G modes and low intensity of disorder-induced D mode of pristine CNTs [Fig. 2(b) and Table I] indicate their high quality.

Increase in D-mode intensity, appearance of D′-mode, significant decrease in 2D mode, increase in G and 2D mode FWHMs (full width at half maximum), and absence of RBM mode are observed upon oxidation and further hydrothermal reduction of the CNTs, which may be associated with their significant structural destruction [Fig. 2(b)]. This is in agreement with IR spectroscopy data. The variation of G/D and G/D′ intensity ratios is summarized in Table I.

Although the duration of hydrothermal treatment does not seem to affect the vibrational spectra and UV/visible absorbance of the resulting products, the electrical resistance of the samples reduced during 1 and 4 h differs. Table II shows the resistivity of the CNT films before and after modification. As expected, electrical resistance of the CNT films supported on insulating substrates significantly decreased after oxidation, while subsequent reduction increases the electrical conductivity due to partial removal of oxygen groups.

Despite the significant decrease in CNT electronic conductivity after chemical treatment, their utilization as a conductive additive is reasonable due to uniform CNT distribution in the sulfur-based composite and much better adhesion. Figure 3(a) shows SEM images of a surface of sulfur/GO composite. Sulfur forms spherical particles of about 900 nm in diameter, which are uniformly covered by a protective GO layer. Comparison of the SEM images in Figs. 3(b)–3(d) reveals that in contrast to pristine CNTs, the chemically modified nanotubes cover sulfur-GO composite much more uniformly. Analysis of the SEM images [Fig. 3(b)] showed that pristine CNTs do not coat "sulfur–GO" particles uniformly due to their high degree of the entanglement, while polar modified CNTs decorate S–GO composite uniformly due to their high affinity with GO layers. Lower magnification SEM images are shown in Supplementary material (Fig. S2).

TABLE I: G/D and G/D′ intensity ratios estimated from Raman spectra fitting.

Sample	G/D	G/D′
Pristine CNTs	28.77	...
Oxidized CNTs	0.77	2.17
Oxidized CNTs after 1 h reduction	0.98	4.95
Oxidized CNTs after 4 h reduction	1.01	5.27

TABLE II: Effect of modification on CNTs resistivity.

Sample	Resistivity, Ohm cm
CNTs	0.38
Oxidized CNTs	$<10^{10}$
Oxidized CNTs after 1 h reduction	260
Oxidized CNTs after 4 h reduction	196

We determined the content of sulfur in S–GO composite using thermogravimetric analysis (TGA), combined with differential scanning calorimetry (DSC) and mass spectrometry (MS) of gas phase products (SO_2) [Fig. 4(a)]. In this case, the opportunity to analyze the MS data makes possible to exclude the effect of GO reduction. Calibration curve for the determination of sulfur in composites was constructed from the values of MS peak area for SO_2 and corresponding known loaded mass of pristine sulfur. It was based on six experimental points and linearized by calibration curve $y = 1.8 \times 10^{-8} \times x$, where x is the sulfur content (mg), with high $R^2 = 0.98$ [Fig. 4 (b)]. The elemental analysis revealed that the composite contained ~73 wt% of sulfur (with ~15 wt% of GO and ~12 wt% of Triton X-100).

Fig. 5 shows the results of electrochemical testing of the electrodes with pristine (a) and modified CNTs (b, c). The discharge voltage profiles of the cells with modified CNTs as a conductive additive demonstrate typical plateaus at nearly 2.3 and 2.1 V, which are ascribed to the conversion of sulfur to higher order lithium polysulfides (Li_2S_8 and Li_2S_4) and Li_2S_4 to

https://doi.org/10.1557/jmr.2019.6 Published online by Cambridge University Press

© Materials Research Society 2019

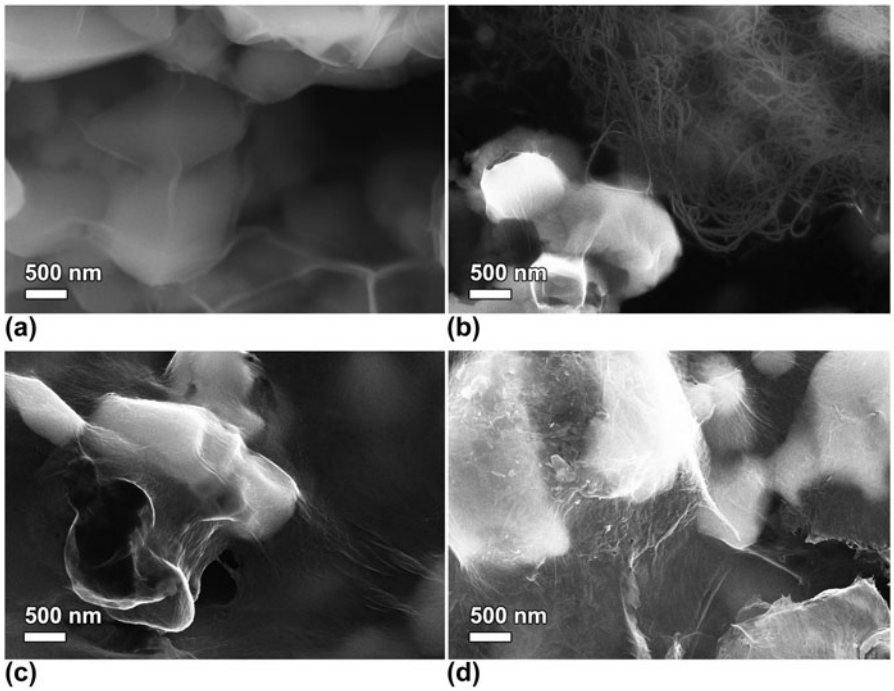


Figure 3: SEM characterization of (a) sulfur–GO composite, (b) electrode coatings based on S–GO composite and pristine CNTs, and (c) CNTs after 1 and (d) 4 h of hydrothermal reduction.

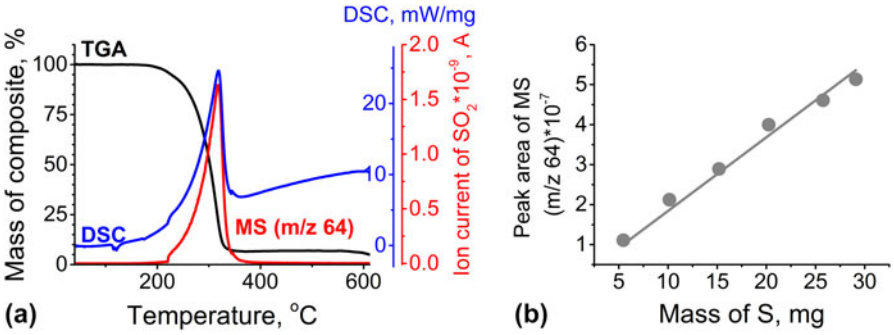


Figure 4: (a) TGA and DSC curves, combined with MS of gas phase products (SO_2) of TGA of sulfur–GO composite, and (b) calibration curve of peak area of MS peak of SO_2 for pristine sulfur.

lower-order lithium polysulfides (Li_2S_3, Li_2S_2) and Li_2S, respectively. Absence of plateau at 2.3 V and lower value of second plateau at 2 V for the cell with pristine CNT-based conductive additive reveal hindered transport of charge that could be explained by nonuniform CNT distribution in the electrode coating structure. This leads to poor sulfur reduction to lithium octasulfide and then to lithium tetrasulfide and as a result to a low length of high-voltage curve (near 80 mA h/g) and low capacity delivered at high-voltage (near 140 mA h/g). Fig. 5 demonstrates that using modified CNTs allows to increase the utilization of sulfur in the cathode more than twice compared with pure CNTs. The lengths of high-voltage plateau and low-voltage plateau of the samples with modified CNTs after reduction for 4 h are 1.4 and 1.9 times higher than for 1 h. The 1.5 times difference in specific capacity of the samples with modified CNTs after 1 and 4 h reduction can be associated with the difference in conductivity of carbon additive that is supported by four-probe electrical measurements (Table II). This indicates that polar nature of modified CNT-based conductive additive combined with appropriate electrical conductivity can dramatically improve specific capacity of the cells in contrast to pristine CNTs.

Cycling performance of the cells with modified CNTs after 4 h hydrothermal reduction as conductive additive is illustrated in Fig. 6. The cycling stability of cathodes with pristine CNTs as well as modified CNTs after 1 and 4 h of hydrothermal reduction is shown in Supplementary material (Fig. S3). Fading of the electrode specific capacity from the 1st to 2nd cycles

https://doi.org/10.1557/jmr.2019.6 Published online by Cambridge University Press

© Materials Research Society 2019

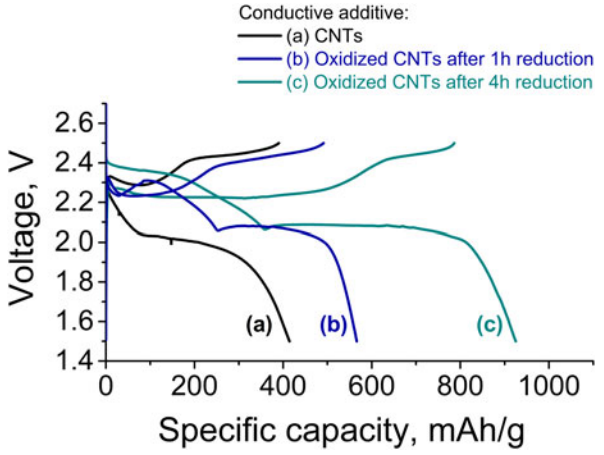


Figure 5: Galvanostatic charge/discharge curves after 1st cycle of the electrodes based on sulfur–GO composite with different conductive additives: (a) CNTs and CNTs after (b) 1 and (c) 4 h of hydrothermal reduction.

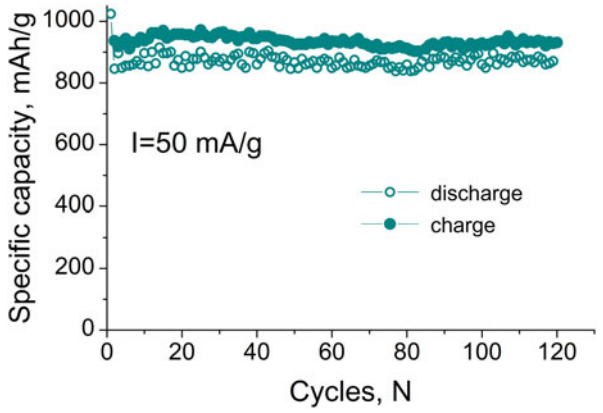


Figure 6: Cycling performances of the electrodes based on sulfur–GO composite with modified CNTs after 4 h of hydrothermal reduction as conductive additive at a current density of 50 mA/g (calculated per 1 g of electrode coating).

(Figs. 6 and S3) is determined by the reduction of the electrolyte due to the reaction with Li anode [32]. After first cycles, the cathodes exhibited good cycling stability due to the passivation of Li anode by $LiClO_4$ as well as ability of GO to suppress shuttle effect [33]. The specific capacity of the electrodes cycled at current density of 50 mA/g (calculated per 1 g of electrode coating) still retained after 120 cycles. We further discuss the role of GO in electrochemical behavior of investigated electrodes. First, as known from literature, GO exhibits irreversible reduction in aprotic electrolytes [34, 35]. According to IR spectroscopy, this reduction is partial and some stable oxygen groups still remain during cycling. The control of oxygen functionalities is important for the sulfur-based cathode to suppress shuttle effect [33]. We performed electrochemical testing of pristine GO-based electrodes in 1 M solution of $LiClO_4$ in tetramethylene sulfone in voltage range of 0–2.5 V. Cyclic voltammetry demonstrated that during the 1st cycle, the cathodic current passed through the electrode of GO in the 1.5–2.5 V range vs. Li^+/Li is less than 1 mA h/g, while expansion of the voltage range from 1.5 to 0 V vs. Li^+/Li leads to the significant increase in cathodic current into 2 orders (Fig. S4). Electrochemical reduction of GO in the 1.5–2.5 V range does not lead to visible change in IR spectra of GO compared with pristine one while extending the range to lower potentials results in almost complete elimination of carboxyl and hydroxyl groups and intercalated and adsorbed water and significant decrease in the intensity of the lines ascribed to carbonyl and ether stretching vibrations (Fig. S5). So the contribution of the irreversible redox of GO in the range of 1.5–2.5 V to the capacity of sulfur–GO-based cathode as well as to the reduction of a number of oxygen functional groups is negligible. Second, the polar nature of GO facilitates efficient interaction between sulfur–GO composite and chemically modified CNTs. Therefore, electrodes based on sulfur–GO composite and modified CNTs as a conductive additive may be promising candidates for the preparation of nontoxic and cost-effective water-based cathode slurries for lithium–sulfur batteries.

Conclusions

In summary, we chemically modified CNTs, which can be used as a conductive additive for the lithium–sulfur battery cathode slurry preparation. The adhesion between conductive carbon additive and the sulfur-containing active material (composite of GO and sulfur particles) was successfully enhanced by enabling a polar interaction between the components. It is worth noting that such approach also enables using water-based binders for cathode slurry preparation in water since modified CNTs are well wetted by water. Despite the decrease in CNT electronic conductivity after chemical treatment, the presence of structural defects and surface groups provides uniform CNT distribution in the sulfur-based composite, which results in more than twice higher electrode specific capacity compared with the electrodes comprising pristine CNTs. These results indicate that chemically modified CNTs are promising conductive additive for the preparation of nontoxic and cost-effective water-based cathode slurries for lithium–sulfur batteries.

Experimental

Synthesis of GO

GO was synthesized by the modified Hummers' method [36]. Three grams of graphite (thermally expanded graphite, SGL Carbon, Wiesbaden, Germany) was placed in a flask with 540 mL of concentrated H_2SO_4 and 60 mL of concentrated

https://doi.org/10.1557/jmr.2019.6 Published online by Cambridge University Press

© Materials Research Society 2019

H_3PO_4, and the mixture was allowed to stand for 30 min at about room temperature with gentle stirring by a top-drive mixer. Eighteen grams of $KMnO_4$ (RUSHIM, Moscow, Russia, purity 99%) was gradually added for about 60 min with gentle stirring, and the obtained mixture was stirred at 50 °C during 24 h. Thirty grams of oxalic acid was added to reduce Mn^{4+} (MnO_2) to Mn^{2+} ($MnSO_4$). The obtained liquid was added to 400 mL of 5 wt% H_2SO_4 aqueous solution for 20 min with stirring, and the resultant mixture was further stirred for 40 min. The resultant mixture was subjected to multiple centrifugation and washing with distilled water until pH 4, and then, the mixture was purified by dialysis in distilled water for 30 days.

Synthesis of sulfur-based composite

Synthesis of sulfur-based composite involved the precipitation of elemental sulfur on GO particles (S–GO) [33]. 8.82 g of $Na_2S_2O_3{\cdot}5H_2O$ (RUSHIM, Moscow, Russia, purity 99%) was dissolved in 940 mL of DI water to which 11.25 mL of 1% Triton X-100 (Sigma-Aldrich, St. Louis, Missouri, for molecular biology) and 150 mg of GO were added. The solution was heated at ~50 °C and then 45 mL of HCl was added to the obtained mixture. The temperature was controlled by a thermometer. The resulting mixture was left with constant stirring for 10 min. The product was washed from acid by using multiple centrifugation and washing with deionized water until pH 7. The S–GO composite was freeze-dried (3 Pa, −55 °C).

CNT chemical modification

Oxidation of pure CNTs has been carried out using modified Hummers' method [20]. 1.5 g of single-walled CNTs (OCSiAl, Novosibirsk, Russia) was placed in a flask with 360 mL of concentrated H_2SO_4 and 40 mL of concentrated H_3PO_4, and the mixture was allowed to stand for 30 min at about room temperature with gentle stirring by a top-drive mixer. Six grams of $KMnO_4$ (RUSHIM, Moscow, Russia, purity 99%) was gradually added for about 20 min with gentle stirring, and the obtained mixture was stirring at 50 °C during 24 h. Ten grams of oxalic acid was added to reduce Mn^{+4} (MnO_2) to Mn^{2+} ($MnSO_4$). The obtained liquid was added to 400 mL of 5 wt% H_2SO_4 aqueous solution for 20 min with stirring, and the resultant mixture was further stirred for 40 min. The resulting mixture of oxidized CNT was subjected to multiple centrifugation and washing with distilled water until pH 4, and then, the mixture was purified by dialysis in distilled water for 30 days.

In order to partially remove oxygen groups from the CNT surface and increase its electronic conductivity, solution of the oxidized CNTs has been hydrothermally treated. For this purpose, 25 mL of slurry with oxidized CNTs (7 mg/mL) was placed in a 30 mL Teflon-lined autoclave and treated at 180 °C for 1 and 4 h.

Structural analysis

Microstructure of the samples was analyzed using a scanning electron microscope Carl Zeiss Supra 40, Oberkochen, Germany. Presence of oxygen groups on the CNT surface was detected by means of transmittance IR spectroscopy in a range of 400–4000 cm^{-1} (Frontier Perkin Elmer, Waltham, Massachusetts) reflection and UV absorption spectroscopy (Perkin Elmer, Waltham, Massachusetts). Raman spectra were acquired with a Renishaw InVia Reflex Spectrometer, Wotton-under-Edge, Gloucestershire, UK using a 633 nm wavelength Ar^+ laser with a power of about 3 mW. Spectral resolution was estimated as of 0.8 cm^{-1}. Analysis of spectral data was carried out using Wire 3.4 Renishaw software, Wotton-under-Edge, Gloucestershire, UK. Raman spectra were fitted by pseudo-Voigt functions to extract the intensities of D, G, D′, and 2D peaks.

Elemental analysis

The content of sulfur in S–GO composite was determined by TGA using NETZCH STA 409 PC Luxx, Selb, Germany, combined with DSC and MS of TGA gas phase products (SO_2) using QMS 403 Aeolos, Selb, Germany. The MS peaks were fitted by Gauss function to extract peak area. Measurements were performed at a heating rate of 10 K/min under air atmosphere.

Electrochemical measurements

Working electrodes were prepared by casting a slurry using doctor blade onto a 20-μm-thick carbon-coated Al foil (Gelon, Lanshan District LinYi City, China). Aqueous slurry for casting was prepared by mixing S–GO composite, carbon additive, and a binder based on acrylonitrile multi-copolymer (LA133; Lanshan District LinYi City, China) in ratio 90%:5%:5%, respectively. Pure CNTs and CNTs after 1 and 4 h of hydrothermal reduction were used as a carbon additive. Electrodes were dried at 80 °C for 5 h in air. The prepared samples were cut into 15-mm disks and then kept in vacuum at 110 °C for 30 min. The typical electrode areal mass loading was about 2 mg/cm^2, and the mass of loaded sulfur was about 1.3 mg/cm^2.

Electrochemical tests of the electrodes based on sulfur–GO composite with different conductive additives were performed in two-electrode configuration in 2032 coin cells. Metallic lithium served as a counter electrode. Working and counter electrodes were separated by a single-layer polypropylene separator (Celgard 2500, Charlotte, North Carolina). 1 M solution of $LiClO_4$ (Sigma-Aldrich, St. Louis, Missouri, battery grade) in tetramethylene sulfone (Alfa Aesar, Ward Hill,

https://doi.org/10.1557/jmr.2019.6 Published online by Cambridge University Press

© Materials Research Society 2019

Massachusetts, purity 99%) [37] was employed as an electrolyte. The amount of electrolyte was 70 μL, with a volume accuracy of ±5% in all test cells. Electrolyte humidity was controlled by Karl Fischer titration (Metrohm KF 831 Coulometer, Herisau, Switzerland) and did not exceed 10 ppm. Cycling was carried out in galvanostatic regime in voltage range of 1.5–2.5 V at a current density of 50 mA/g (calculated per 1 g of composite).

0.1 mL of 1 mg/mL methanol-based sol of GO was spin-coated at 1000 rpm on Al foil. Electrochemical testing of GO-based electrodes was performed in three-electrode cell in the same electrolyte in potential range of 0–2.5 V vs. Li^+/Li. Metallic Li served as a reference electrode, Pt as a counter electrode, and GO-based film on Al foil as a working electrode.

Electrical conductivity of CNT-based films before and after chemical modification was measured by four-probe method (Jandel, Linslade, United Kingdom, RMS-EL-Z). Films were prepared by airbrushing CNT based sols (3 mg/mL) in NMP (RUSHIM, Moscow, Russia, 99%, preliminary distilled under vacuum) onto glass substrates. NMP was chosen as a solvent due to high aggregation of pure CNT in aqueous solutions. The thickness of deposited films was near 20 μm and controlled by micrometer screw gauge with an accuracy of 2.54 μm.

Associated content

Supplementary material contains additional IR spectra of modified CNTs and IR spectra in full scale (Fig. S1) and lower magnification SEM images of electrode coatings based on S–GO composite with pristine and modified CNTs (Fig. S2). Electrochemical characterization of the electrodes based on sulfur–GO composite with different conductive additives: CNTs and CNTs after 1 and 4 h hydrothermal reduction (Fig. S3). Analysis of the redox of GO in the potential range of lithium–sulfur batteries (Fig. S4) and IR spectra of GO before and after the redox (Fig. S5).

Acknowledgments

This work was supported by the Russian Foundation for Basic Research (RFBR No. 16-33-60229). D.M.I. acknowledges financial support from the Russian Science Foundation (No. 16-42-01093). We thank Dr. S.G. Dorofeev for discussion of IR measurements. This work was performed using equipment purchased within the Program of Development of the Lomonosov Moscow State University.

Supplementary material

To view supplementary material for this article, please visit https://doi.org/10.1557/jmr.2019.6.

References

1. **Q. Pang, X. Liang, C.Y. Kwok, and L.F. Nazar**: Advances in lithium–sulfur batteries based on multifunctional cathodes and electrolytes. *Nat. Energy* **1**, 1 (2016).
2. **X.L. Ji and L.F. Nazar**: Advances in Li–S batteries. *J. Mater. Chem.* **20**, 9821 (2010).
3. **D.A. Nole and V. Moss**: Battery employing lithium–sulphur electrodes with non-aqueous electrolyte. U.S. Patent No. 3532543, 1 (1968).
4. **M.K. Song, E.J. Cairns, and Y. Zhang**: Lithium/sulfur batteries with high specific energy: Old challenges and new opportunities. *Nanoscale* **5**, 2186 (2013).
5. **R.D. Rauh, F.S. Shuker, J.M. Marston, and S.B. Brummer**: Formation of lithium polysulfides in aprotic media. *J. Inorg. Nucl. Chem.* **39**, 1761 (1977).
6. **Y.V. Mikhaylik and J.R. Akridge**: Polysulfide shuttle study in the Li/S battery system. *J. Electrochem. Soc.* **151**, A1969 (2004).
7. **H. Yamin, A. Gorenshtein, J. Penciner, Y. Sternberg, and E. Peled**: Lithium sulfur battery—Oxidation reduction-mechanisms of polysulfides in THF solutions. *J. Electrochem. Soc.* **135**, 1045 (1988).
8. **Q. Pang, D. Kundu, M. Cuisinier, and L.F. Nazar**: Surface-enhanced redox chemistry of polysulphides on a metallic and polar host for lithium–sulphur batteries. *Nat. Commun.* **5**, 1 (2014).
9. **J.W. Zhou, R. Li, X.X. Fan, Y.F. Chen, R.D. Han, W. Li, J. Zheng, B. Wang, and X.G. Li**: Rational design of a metal-organic framework host for sulfur storage in fast, long-cycle Li–S batteries. *Energy Environ. Sci.* **7**, 2715 (2014).
10. **Z.X. Zhao, S. Wang, R. Liang, Z. Li, Z.C. Shi, and G.H. Chen**: Graphene-wrapped chromium-MOF(MIL-101)/sulfur composite for performance improvement of high-rate rechargeable Li–S batteries. *J. Mater. Chem. A* **2**, 13509 (2014).
11. **Z.Q. Wang, B.X. Wang, Y. Yang, Y.J. Cui, Z.Y. Wang, B.L. Chen, and G.D. Qian**: Mixed-metal-organic framework with effective Lewis acidic sites for sulfur confinement in high-performance lithium–sulfur batteries. *ACS Appl. Mater. Interfaces* **7**, 20999 (2015).
12. **X. Liang, C. Hart, Q. Pang, A. Garsuch, T. Weiss, and L.F. Nazar**: A highly efficient polysulfide mediator for lithium–sulfur batteries. *Nat. Commun.* **6**, 5682 (2015).
13. **L.C.H. Gerber, P.D. Frischmann, F.Y. Fan, S.E. Doris, X. Qu, A.M. Scheuermann, K. Persson, Y.M. Chiang, and B.A. Helms**: Three-dimensional growth of Li_2S in lithium–sulfur batteries promoted by a redox mediator. *Nano Lett.* **16**, 549 (2016).
14. **S. Meini, R. Elazari, A. Rosenman, A. Garsuch, and D. Aurbach**: The use of redox mediators for enhancing utilization of Li_2S cathodes for advanced Li–S battery systems. *J. Phys. Chem. Lett.* **5**, 915 (2014).

https://doi.org/10.1557/jmr.2019.6 Published online by Cambridge University Press

© Materials Research Society 2019

15. **H.J. Peng, J.Q. Huang, X.B. Cheng, and Q. Zhang**: Review on high-loading and high-energy lithium–sulfur batteries. *Adv. Energy Mater.* **7**, 1 (2017).
16. **G.M. Zhou, L.C. Yin, D.W. Wang, L. Li, S.F. Pei, I.R. Gentle, F. Li, and H.M. Cheng**: Fibrous hybrid of graphene and sulfur nanocrystals for high-performance lithium–sulfur batteries. *ACS Nano* **7**, 5367 (2013).
17. **H.W. Chen, C.H. Wang, Y.F. Dai, S.Q. Qiu, J.L. Yang, W. Lu, and L.W. Chen**: Rational design of cathode structure for high rate performance lithium–sulfur batteries. *Nano Lett.* **15**, 5443 (2015).
18. **L.C. Zeng, F.S. Pan, W.H. Li, Y. Jiang, X.W. Zhong, and Y. Yu**: Free-standing porous carbon nanofibers–sulfur composite for flexible Li–S battery cathode. *Nanoscale* **6**, 9579 (2014).
19. **W.M. Kang, N.P. Deng, J.G. Ju, Q.X. Li, D.Y. Wu, X.M. Ma, L. Li, M. Naebe, and B.W. Cheng**: A review of recent developments in rechargeable lithium–sulfur batteries. *Nanoscale* **8**, 16541 (2016).
20. **D.V. Kosynkin, A.L. Higginbotham, A. Sinitskii, J.R. Lomeda, A. Dimiev, B.K. Price, and J.M. Tour**: Longitudinal unzipping of carbon nanotubes to form graphene nanoribbons. *Nature* **458**, 872 (2009).
21. **L.W. Ji, M.M. Rao, H.M. Zheng, L. Zhang, Y.C. Li, W.H. Duan, J.H. Guo, E.J. Cairns, and Y.G. Zhang**: Graphene oxide as a sulfur immobilizer in high performance lithium/sulfur cells. *J. Am. Chem. Soc.* **133**, 18522 (2011).
22. **L. Zhang, L.W. Ji, P.A. Glans, Y.G. Zhang, J.F. Zhu, and J.H. Guo**: Electronic structure and chemical bonding of a graphene oxide–sulfur nanocomposite for use in superior performance lithium–sulfur cells. *Phys. Chem. Chem. Phys.* **14**, 13670 (2012).
23. **J.P. Rong, M.Y. Ge, X. Fang, and C.W. Zhou**: Solution ionic strength engineering as a generic strategy to coat graphene oxide (GO) on various functional particles and its application in high-performance lithium–sulfur (Li–S) batteries. *Nano Lett.* **14**, 473 (2014).
24. **G. He, C.J. Hart, X. Liang, A. Garsuch, and L.F. Nazar**: Stable cycling of a scalable graphene–encapsulated nanocomposite for lithium–sulfur batteries. *ACS Appl. Mater. Interfaces* **6**, 10917 (2014).
25. **M. He, L-X. Yuan, W-X. Zhang, X-L. Hu, and Y-H. Huang**: Enhanced cyclability for sulfur cathode achieved by a water-soluble binder. *J. Phys. Chem. C* **115**, 15703 (2011).
26. **Z. Zhang, W. Bao, H. Lu, M. Jia, K. Xie, Y. Lai, and J. Li**: Water-soluble polyacrylic acid as a binder for sulfur cathode in lithium–sulfur battery. *ECS Electrochem. Lett.* **1**, 34 (2012).
27. **M-K. Song, Y. Zhang, and E.J. Cairns**: A long-life, high-rate lithium/sulfur cell: A multifaceted approach to enhancing cell performance. *Nano Lett.* **13**, 5891–5899 (2013).
28. **T. Szabó, O. Berkesi, P. Forgó, K. Josepovits, Y. Sanakis, D. Petridis, and I. Dékány**: Evolution of surface functional groups in a series of progressively oxidized graphite oxides. *Chem. Mater.* **18**, 2740 (2006).
29. **E. Pretsch, P. Bühlmann, and M. Badertscher**: *Structure Determination of Organic Compounds. Tables of Spectral Data* (Springer, Berlin, Heidelberg, Germany, 2009); pp. 245–312.
30. **D. Li, M.B. Muller, S. Gilje, R.B. Kaner, and G.G. Wallace**: Processable aqueous dispersions of graphene nanosheets. *Nat. Nanotechnol.* **3**, 101 (2008).
31. **M.S. Dresselhaus, G. Dresselhaus, R. Saito, and A. Jorio**: Raman spectroscopy of carbon nanotubes. *Phys. Rep.* **409**, 47 (2005).
32. **V.S. Kolosnitsyn, E.V. Karaseva, E.V. Kuzmina, and A.L. Ivanov**: Why the amount of electrolyte affects the characteristics of lithium–sulfur cells. *Elektrokhimiya* **52**, 315 (2016).
33. **H.L. Wang, Y. Yang, Y.Y. Liang, J.T. Robinson, Y.G. Li, A. Jackson, Y. Cui, and H.J. Dai**: Graphene-wrapped sulfur particles as a rechargeable lithium-sulfur battery cathode material with high capacity and cycling stability. *Nano Lett.* **11**, 2644 (2011).
34. **Y. Harimaa, S. Setodoia, I. Imaea, K. Komaguchia, Y. Ooyamaa, J. Ohshitaa, H. Mizotab, and J. Yano**: Electrochemical reduction of graphene oxide in organic solvents. *Electrochim. Acta* **56**, 5363 (2011).
35. **J. Kauppilaa, P. Kunnasa, P. Damlina, A. Viinikanojaa, and C. Kvarnström**: Electrochemical reduction of graphene oxide films in aqueous and organic solutions. *Electrochim. Acta* **89**, 84 (2013).
36. **D.C. Marcano, D.V. Kosynkin, J.M. Berlin, A. Sinitskii, Z. Sun, A. Slesarev, L.B. Alemany, W. Lu, and J.M. Tour**: Improved synthesis of graphene oxide. *ACS Nano* **4**, 4806 (2010).
37. **V.S. Kolosnitsyn, E.V. Kuzmina, and E.V. Karaseva**: On the reasons for low sulphur utilization in the lithium–sulphur batteries. *J. Power Sources* **274**, 203 (2015).

https://doi.org/10.1557/jmr.2019.6 Published online by Cambridge University Press

© Materials Research Society 2019